Geophysical Research Letters

Supporting Information for

Investigating Subsurface Pathways of Fukushima Cesium in the Northwest Pacific

Ella R. Cedarholm[1], Irina I. Rypina[2], Alison M. Macdonald[2] and Sachiko Yoshida[2]
[1]University of New Hampshire, Durham, NH 03824
[2]Woods Hole Oceanographic Institution, Woods Hole, MA 02543

Contents of this file:

Text S1 to S4

Figures S1 to S6

Additional Supporting Information (Files uploaded separately):

Caption for Movie S1 (ms01.avi)

Introduction

Supporting text provides further detail on the methods used for model validation, velocity and trajectory calculation and data processing described in the manuscript text. Accompanying figures referenced in the supporting text are .png and .jpg files. The AVI video file contains 770 frames at 10fps. The video was created using MATLAB's VideoWriter (© 1984–2019 The MathWorks, Inc.). Trajectory velocities and surface densities were calculated using HYCOM GLBa0.08 expt_90.0v output (see main text for links).

Text S1. Validation of HYCOM Output:

A high-resolution data-assimilating numerical model may be the best estimate of basin-scale subsurface ocean circulation presently available. That being said, one would still like to know how well the model output resembles observed "reality". HYCOM assimilates satellite altimeter observations, satellite and in situ sea surface temperature, as well as available in situ vertical temperature and salinity profiles from XBTs, CTDs, floats, drifters and moored buoys (https://www.hycom.org and the many references cited therein, e.g. Cummings & Smedstad, 2013). As many of the observations to which we could compare have been used in the assimilation, comparison with these data does not necessarily validate the model but rather provides information on how important the model considered the input observations to the state estimate.

Comparison between annual mean and synoptic potential densities from HYCOM and the CLIVAR P02 zonal hydrographic line (Figure 2) provided confirmation of agreement in the shape and depth of the zonal density field along 30°N (Section 3.1). Figure S1 provides similar confirmation along the Jan.-Feb. 2012 CLIVAR meridional P10 section at 145°E. As in the zonal comparison, the "instantaneous" snapshot provided by the hydrography (S1a) is noisier and has deeper mixed layers than the 2012 mean HYCOM field (S1b), but the density range, depth and shape of the isopycnals are similar. The exception is the region of outcrop in the north, which the hydrographic line (a) captures because it was occupied during the winter season of strong mixing and mode water formation. The model-observation agreement is further supported by the "synoptic" model section (S1c, created by sampling the model at the time and location of the observations) where the resemblance both in the vertical and horizontal between the density field and the observations during these winter months in clear.

To validate the model output on a broader scale, the depth of the $26.5\sigma_\theta$ surface in HYCOM was compared to that calculated from a gridded Argo product, ISAS-15 (https://www.seanoe.org; Kolodziejczyk et al., 2017; Gaillard et al., 2016) and in situ individual Argo float profile temperatures and salinities (http://www.argodatamgt.org). The depth of $26.5\sigma_\theta$ in the 0.5° gridded ISAS-15 product (not shown) produces, not surprisingly, a somewhat fuzzier picture than the 1/12° HYCOM output whether compared over the months of early 2011 or across the full March 2011 to April 2013 period and whether or not the HYCOM output is interpolated to 0.5° grid. Large differences are apparent within the meandering current and strong eddy fields (simply because the exact details of the meanders and eddies are not always well aligned between HYCOM and Argo), but outside this region depth differences were 10-20% of the $26.5\sigma_\theta$ depth. Comparison to in situ Argo profiles was even more favorable. Again, there are large differences (>100 m) in the KE region, where the modeled meanders and eddies do not quite line up with the float profiles (keep in mind that the positions of the profiles themselves are subject to error particularly in fast currents). To estimate the magnitude of the difference outside

the most dynamic regions, we removed extrema (defined as the mean depth differences greater than twice the standard deviation and representing ~6% of the data, i.e. ~1000 out of 17500 profiles) to find an average depth difference of 2±2% or ~9 m out of a range of 400 m (over the entire Northwest Pacific region and two year period of the study). A similar result can be obtained by looking outside the region of the KE (which we defined as 32°-39°N, an area that includes ~30% of the data).

Lastly we looked to understand how well the model produces the "observed" velocity field. One could compare to the gridded Argo absolute geostrophic velocity product AGVA (Gray & Riser, 2014). However, given that HYCOM already assimilates Argo data, that the validation to Argo profiles (above) has been favorable, and that AGVA is presently only available on a 1.0° x 1.0° grid for 2004-2010, the comparison was deemed unhelpful. Instead, we compared the AVISO "allsat" product absolute surface geostrophic velocity estimates to HYCOM surface velocities, first low-pass filtering both products to remove wavelengths less than 14 days and 1 degree (where 1° is ~100 km in the subtropics, or more specifically 111 km of latitude, and of 71 to 104 km of longitude between 20°N and 50°N).

The two representations of March 2011-2013 monthly mean eddy kinetic energy (EKE) are quite similar (Figure S2) as are the maximum EKE estimates. As in the other comparisons, in the region of the strong meandering and evolving current and its associated rich eddy field, small location offsets are responsible for the largest differences between the two products, but overall they agree well in pattern and magnitude. Averaging over all instances of each month between March 2011 and April 2013 (not shown), suggests domain-averaged monthly mean EKE differences of 21±7%. The greatest differences (30%) occur in the dynamic water formation months of February and March and the smallest (7-14%) in May-June. It should also be noted that geographically speaking most of the largest percentage differences contributing to these statistics are attributed not to the region around the KE, but rather to the southern portion of the field (20-28°N) just to the north of North Equatorial Current. EKE values here are generally low in both the HYCOM and AVISO fields, so these are differences between small numbers. Looking to the north of 28°N, the region of interest to this study, the domain-averaged monthly mean EKE difference is 10±7%. Some seasonality still exists. In this northern domain, while the minimum percent differences (1-2%) still occur in May-June, the maximum (18-20%) shifts to July-Sept.

As stated in the text, all the comparisons to observations performed suggest that HYCOM is producing a sensible velocity field as well as the correct depth and shape of the $26.5\sigma_\theta$ surface as they evolve in space and time. At 1/12° it is also fully resolving the mesoscales and capturing some effects of submeso-scale processes on this isopycnal; the latter is well beyond observational capabilities on basin scales.

Text S2. Velocity Calculation and Particle Tracking:

To obtain daily horizontal velocities on the $26.5\sigma_\theta$ density surface, the depth of this surface at each horizontal grid point was first obtained by linearly interpolating potential densities calculated from daily temperature and salinity HYCOM output between March 2011 and April 2013. The daily horizontal *u* and *v* velocities were then linearly interpolated from the original model grid depths to the depth of the $26.5\sigma_\theta$ isopycnal. These time-varying along isopycnal velocities were used to advect the simulated particles. We employed an adaptive variable-step 4th order Runge-Kutta trajectory integration scheme (built-in function "ode45" in MATLAB [© 1984–2019 The MathWorks, Inc.]), where the time step along each trajectory is iteratively chosen to satisfy a prescribed tolerance value (10^{-6} in our case). To implement this integration scheme, HYCOM velocities were interpolated in both time and space using a bi-linear interpolation scheme (from the original fixed spatio-temporal grid of 1/12 deg and 1 day to the variable spatio-temporal stepping along each trajectory). The same integration/interpolation scheme has been used in Rypina et al. (2011; 2013; 2014b; 2019).

Text S3. **Forward Trajectory Simulation:**

Forward particle trajectories were calculated along the $26.5\sigma_\theta$ isopycnal from the date of the FDNPP accident (11 March 2011) and region of maximum atmospheric deposition (Figure 1, purple polygon based on Stohl et al., 2012) to the day of the deepest cesium observation from the 30°N transect (22 April 2013). A fixed staggered release grid spanning the purple polygon was constructed, with 720 release points per square degree area. Trajectories were released only from the interior of the purple polygon and only where and when the tracer had an opportunity to enter the $26.5\sigma_\theta$ water, i.e. where and when the $26.5\sigma_\theta$ isopycnal interacted with (i.e., lay within) the mixed layer computed according to the 0.03 criterion within the polygon. As in the backward trajectory formulation, because the model cannot be expected to reproduce the exact ocean state, trajectories were released from every grid point of the staggered release grid within ± 0.25° and every day within ± three days of the interaction event. Therefore, the releases ran from 8 March 2011 to 20 May 2011. A bar graph of the number of forward releases per day can be seen in Figure S4. As all forward trajectories begin in the polygon during interaction of the $26.5\sigma_\theta$ surface with the mixed layer, they are all considered to represent possible pathways for Cs_F and they were all used to create the full forward probability and arrival date maps (Figures 4c,d).

S3.1 Latitudinally Limited Probability Maps

The estimated region of maximum atmospheric deposition is schematically represented by the purple polygon (Figure 1). This region spans a broad range of ocean dynamics and mixing, including strong, temporally and spatially evolving currents such as the meandering undulating KE current. To better understand how the meandering KE and the permeable barrier near its core affect the fate of the cesium signal, the trajectories from the forward experiment were divided according to the latitude of their release. Releases were evaluated in 0.2° increments of latitude.

It was found that the fate those trajectories that were released at and to the north of 39°N (Figure 4f) differed from that associated with trajectories released at and to the south of 38°N (not

shown, but represented by the difference between panels (d) and (f) of Figure 4). The solid green curve in this figure, derived from a single snapshot of sea surface height and temperature (Isoguchi et al., 2006), represents an example of the location of the north wall of the Kuroshio as it turns away from the coast and KE further east. The dotted green line based on a hydrographic climatology of geostrophic velocities (Isoguchi et al., 2006) is representative of the current core. Together, with the black dots at the locations of releases at and to the north of 39°N, the green curves suggest that these trajectories are generally entering the system to the north of the north wall of the meandering current, whereas trajectories entering south of this may be arriving to the east of Kuroshio where it hugs the coast or to the south of the KE after the current has left the coast. Trajectories that leave from the small purple triangular region to the east of the main purple polygon (triangle best seen in Figure 3) have a tendency to stay to the south of the front (probability map not shown), and when they cross, they do so preferentially between ~150-155°E. However, it should be noted that this last conclusion cannot be considered robust as it is based on very few trajectories (125). A thorough investigation on the fate of water parcels based on their point of entry into this region could be an interesting extension to the present study.

Consistent with the notion of a permeable transport barrier associated with the KE, trajectories released south of 39°N had little difficulty moving southward (broad orange swath to the south of current in Figure 4d), whereas the southward spread of particles released to the north of 39°N was largely impeded by the KE barrier west of 155°-160°E (see greenish colors in Figure 4f in the location where a broad swath of orange is present in Figure 4d). Using a time-evolving KE core instead of a fixed critical latitude of the northernmost KE extent would provide a more thorough investigation of the KE barrier effect; however, such study is beyond the scope of this paper and is left for the future.

Text S4. Extended Acknowledgements:

Funding for the development of HYCOM has been provided by the National Ocean Partnership Program and the Office of Naval Research. Data assimilative products using HYCOM are funded by the U.S. Navy. Computer time was made available by the DoD High Performance Computing Modernization Program. Argo data were collected and made freely available by the International Argo Program and the national programs that contribute to it. (http://www.argo.ucsd.edu, http://argo.jcommops.org). The Argo Program is part of the Global Ocean Observing System.

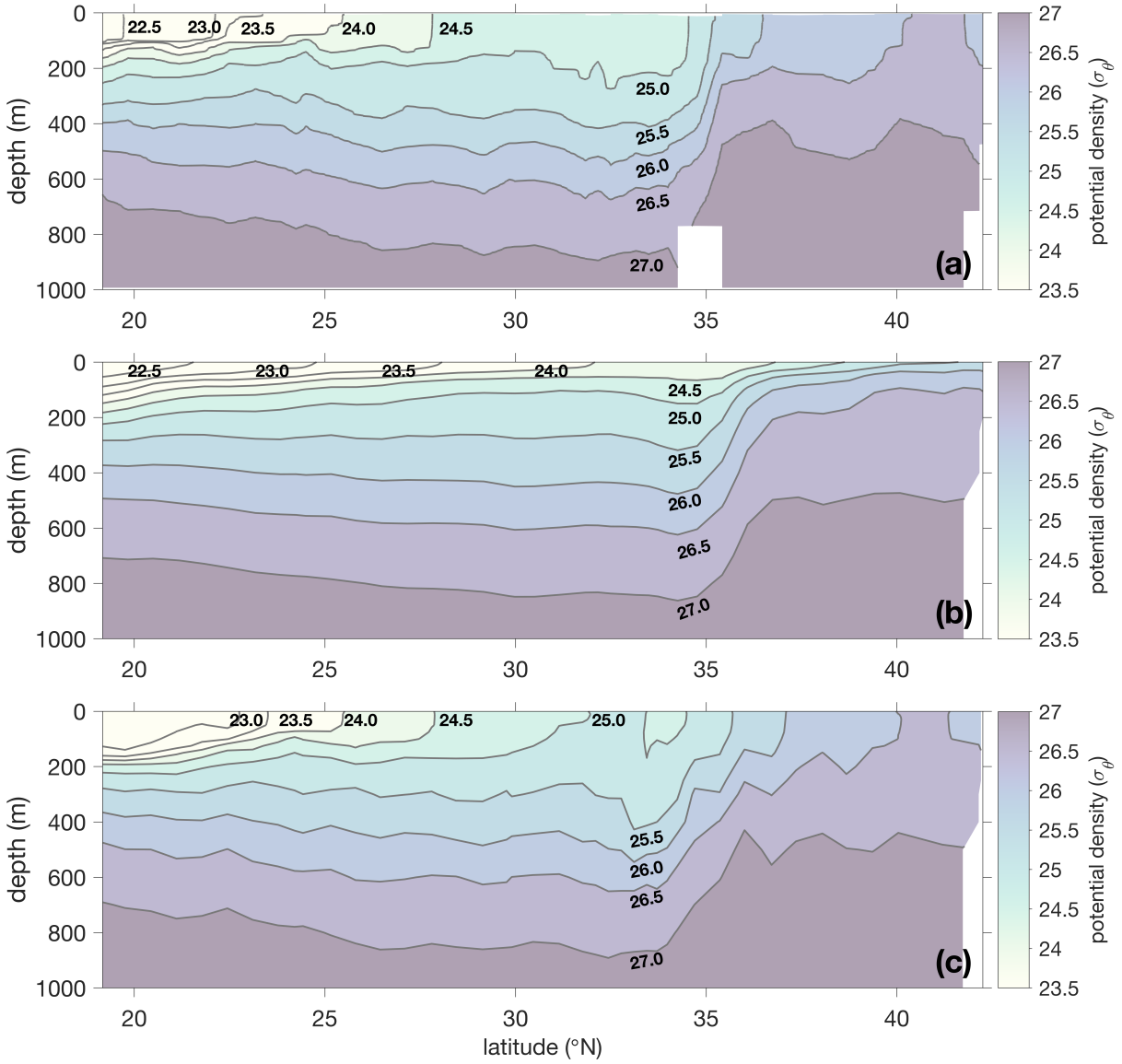

168

169 **Figure S1.** Vertical sections of potential density at 145°E from the surface to 1000 m with
170 isopycnals labeled in bold text. (a) Observed P10 CTD temperature and bottle sample calibrated
171 CTD salinity based densities, (b) 1/12° global HYCOM 2012 mean densities along P10 track,
172 and (c) HYCOM densities sampled at the time and location of the P10 casts.

173

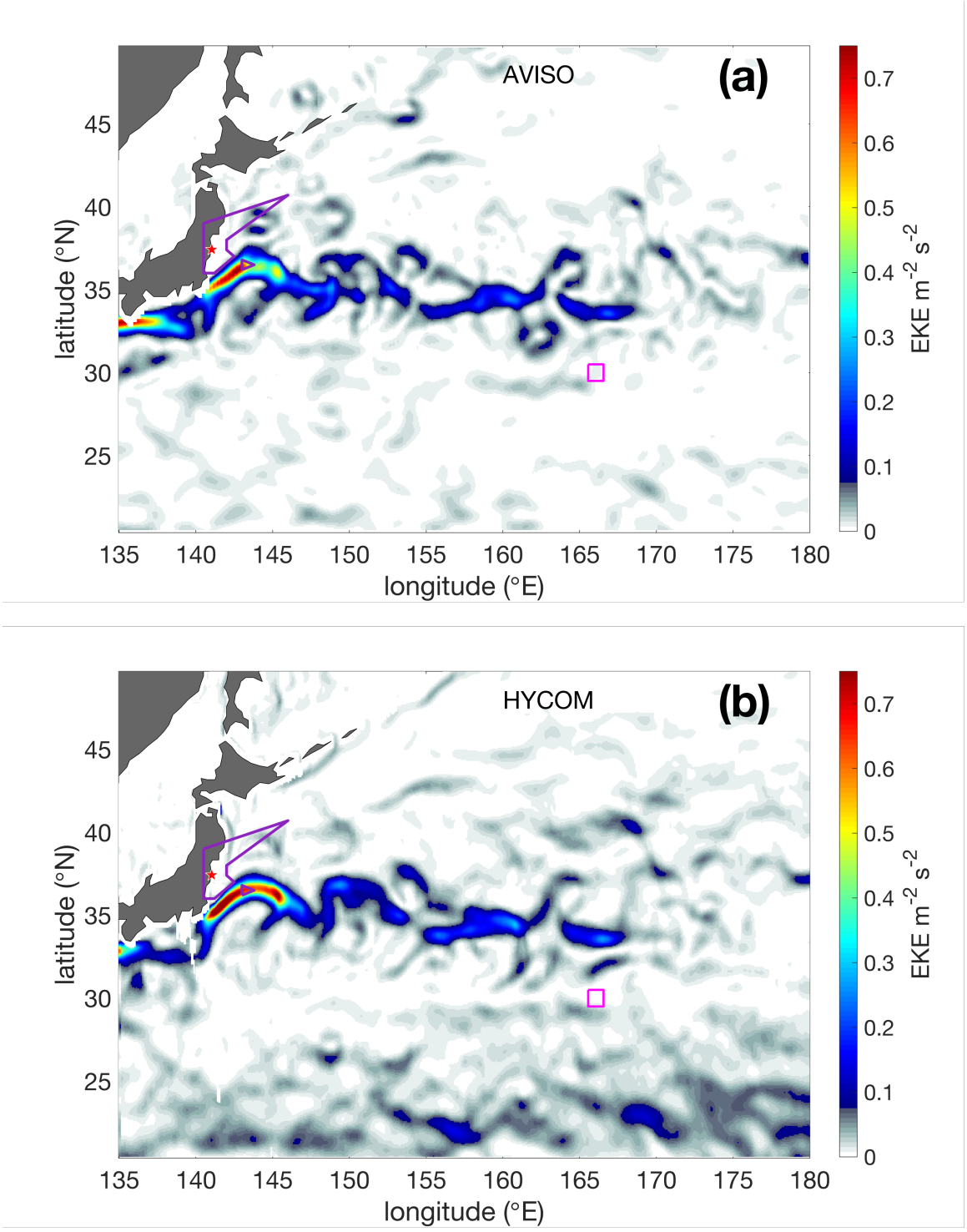

Figure S2. Mean eddy kinetic energy (EKE) of all instantances of the month of March during the study period (March 2011 to April 2013) based on (a) AVISO and (b) HYCOM surface velocity estimates (Units m^2s^{-2}). Pink box, purple polygon and red star indicate the observed deep Cs_F location, the region of maximum atmospheric deposition, and the FDNPP, respectively.

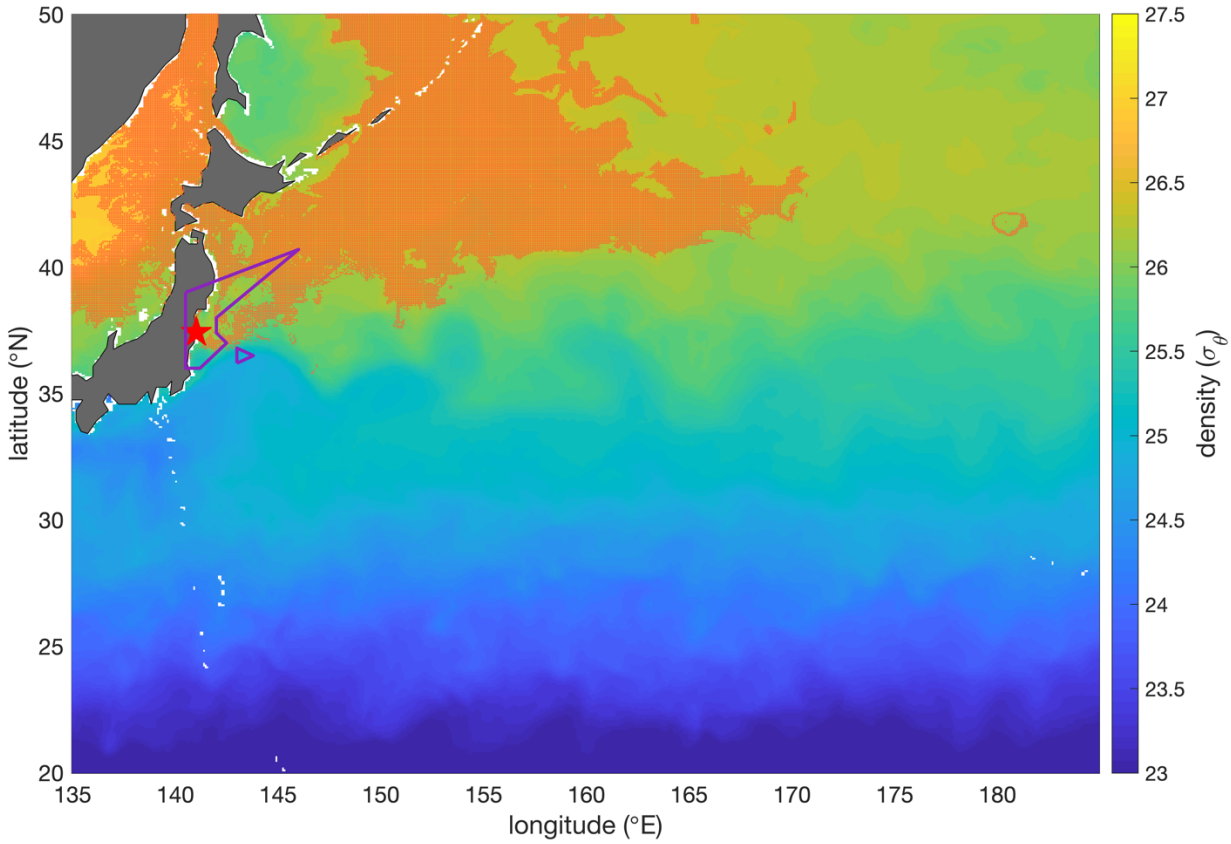

Figure S3: Mean HYCOM surface density between the forward simulation trajectory release dates (8 March 2011 through 20 May 2011) with location of every 26.5σ_θ interaction with the mixed layer indicated by an orange cross. Symbols as in Figure S2.

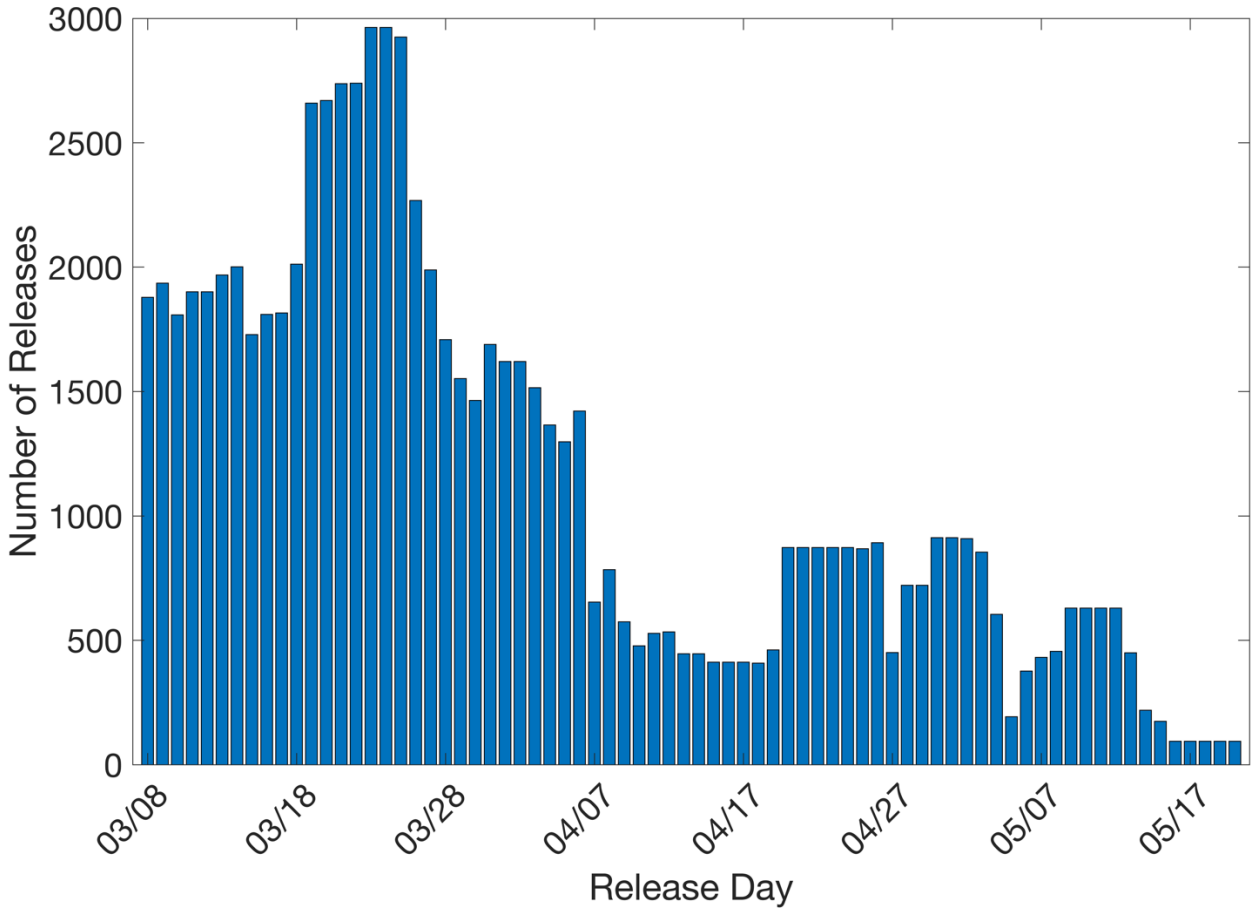

Figure S4: Number of forward trajectory releases over full release period 8 March to 20 May 2011. Each release represents an interaction of the $26.5\sigma_\theta$ isopycnal with the mixed layer within ± three days and ± 0.25° from each fixed grid point in the polygon.

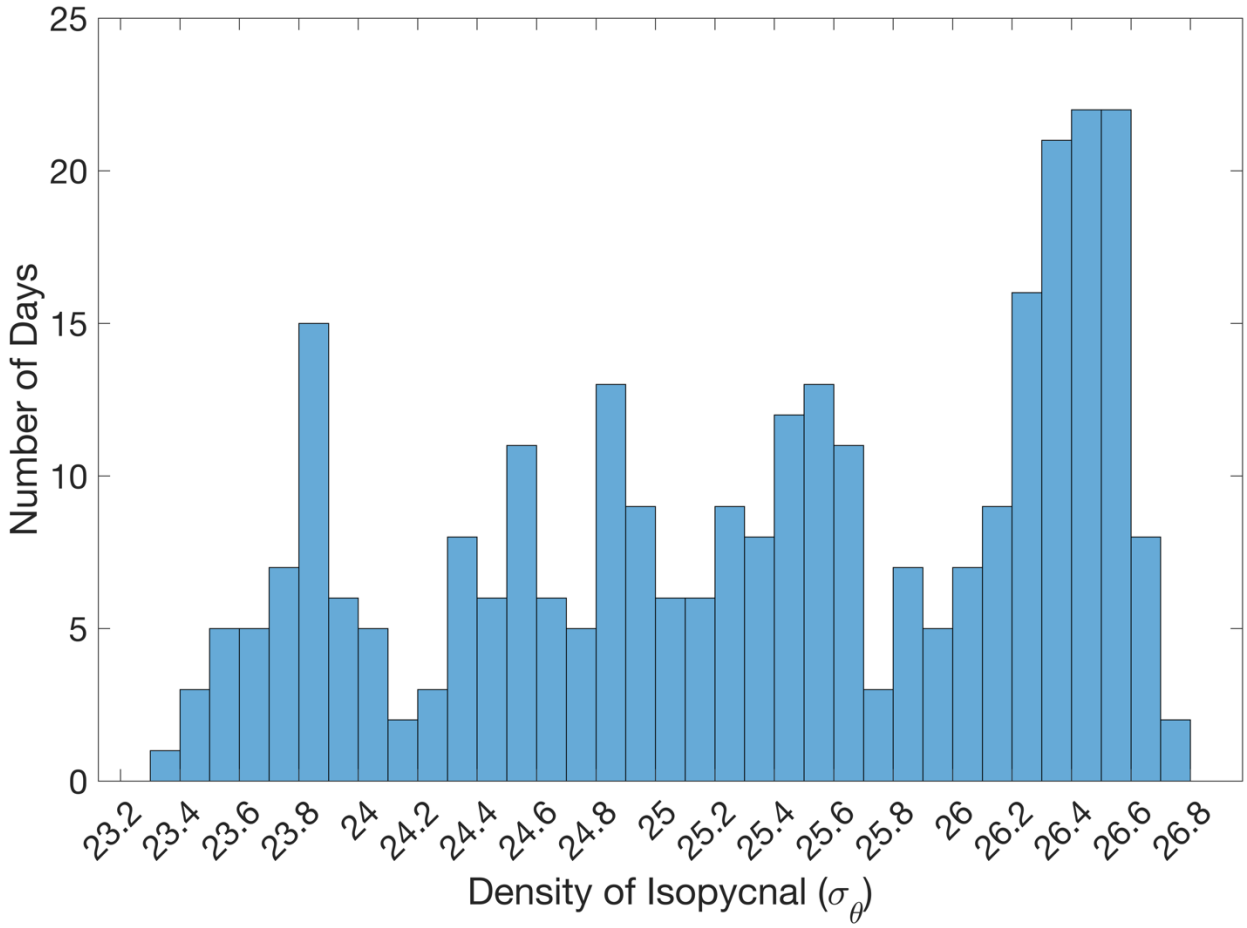

Figure S5: Number of days between 15 March and 31 December 2011 that each 0.25° x 0.25° averaged density represented the maximum reached by the mixed layer in the purple polygon.

Movie S1. Animation of HYCOM surface density (color shading) from 8 March 2011 through 21 April 2013. Blue contour indicating times and locations of densities within ±0.03 kg m^{-3} of $26.5\sigma_\theta$. Symbols as in Figure S2.